Fusion Engineering and Design 85 (2010) 1331–1335

Contents lists available at ScienceDirect

Fusion Engineering and Design

journal homepage: www.elsevier.com/locate/fusengdes

Impact of various plasma instabilities on reliability and performance of tokamak fusion devices

A. Hassanein*, T. Sizyuk, V. Sizyuk, G. Miloshevsky

School of Nuclear Engineering, Purdue University, 400 Central Drive, West Lafayette, IN 47907, USA

ARTICLE INFO

Article history:
Available online 18 April 2010

Keywords:
Disruption
ELM
VDE
Runaway electrons
HEIGHTS

ABSTRACT

Plasma instability events such as disruptions, resulting runaway electrons, edge-localized modes (ELM), and vertical displacement events (VDE) are mainly the most limiting factor for successful tokamak reactor concept. The plasma-facing components (PFC), e.g., wall, divertor, and limited surfaces of a tokamak as well as coolant structure materials are subjected to intense particle and heat loads and must maintain a clean and stable surface environment between them and the core/edge plasma. This is critical to fusion device performance. Comprehensive research efforts are developed utilizing the HEIGHTS simulation package to study self-consistently various effects of high power transient on material operation/selection. The package consists of several models that integrate different stages of plasma–wall interactions starting from energy release at scrape-off-layer and up to the transport of the eroded debris and splashed wall materials as a result of the deposited energy. The integrated model predicts material loss, PFC lifetime from transients, and effects on core plasma performance. HEIGHTS initial simulation shows that a single event such as a major disruption, VDE, or runaway electron could severely damage the reactor wall and structural materials and disrupt operation for a significant time. HEIGHTS is used to identify safer operating window regimes and upper transient limits that PFC can withstand during various instabilities.

1. Introduction

Various damage to plasma-facing components (PFM) as a result of plasma instabilities still remains a major obstacle to a successful tokamak reactor design. Loss of plasma confinements and instabilities take various forms, such as major disruptions, which include both thermal and current quench (sometimes producing runaway electrons); edge-localized modes (ELM), and vertical displacement events (VDE). Most plasma instabilities may cause both surface and bulk damage to plasma-facing and structural materials [1]. Surface damage mainly consists of high erosion losses attributable to surface vaporization, spallation, and melt-layer erosion. Major bulk damage of plasma instabilities, particularly those of longer duration, such as VDE, or those with deeper deposited energy, such as runaway electrons, is the result of the high heat flux reaching the coolant channels, possibly causing burnout of these tubes [2–4]. Additional bulk damage may include large temperature increases in structural materials and at the interfaces between surface coatings and structural materials. These large temperature increases can cause high thermal stresses, melting and detachment of surface coating material, and material fatigue and failure. In addition to these effects, the transport and redeposition of the eroded surface materials to various locations on PFC are of major concern for plasma contamination, safety (dust inventory hazard), and successful and prolonged plasma operation after instability events [5].

The HEIGHTS package has been developed as an instrument and comprehensive tool for the simulation and optimization of the interaction processes during the intense energy deposition of various energy sources such as plasma, laser, and particle beams incident on target materials. The HEIGHTS package has numerous integrated models that follow the early stages of a plasma disruption/giant ELM in the plasma and scrape-off-layer up to the transport of the eroded debris and splashed target materials as a result of the deposited energy. The enhanced transient models include 3D energy deposition and material bulk thermal response, 3D thermal hydraulic analysis of coolant channels, surface melt-layer formation and movement, near-surface vapor-shield formation and evolution, 3D photon line and continuum radiation transport, atomic and molecular processes of surface materials in the plasma, and photon radiation/vapor motion effects on nearby components. Recently, HEIGHTS investigated in detail the effects of plasma instabilities including VDEs [2,6], ELMs [7], disruptions [1,8] and runaway electrons [9] on plasma-facing components (PFC) of a tokamak reactor and analyzed ways for mitigating such effects. The simulation results showed that disruptions and high power ELMs cause excessive target erosion of candidate

* Corresponding author. Tel.: +1 765 496 9731; fax: +1 765 496 2233.
E-mail address: hassanein@purdue.edu (A. Hassanein).

0920-3796/$ – see front matter © 2010 Elsevier B.V. All rights reserved.
doi:10.1016/j.fusengdes.2010.03.039

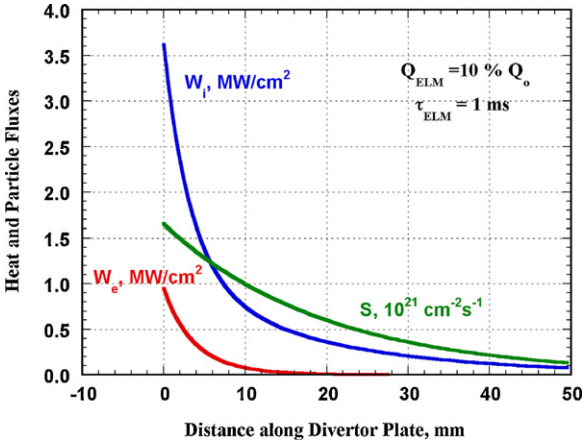

Fig. 1. Calculated spatial distribution of particle flux S, electron heat flux W_e, and ion heat flux W_i during an ELM [12].

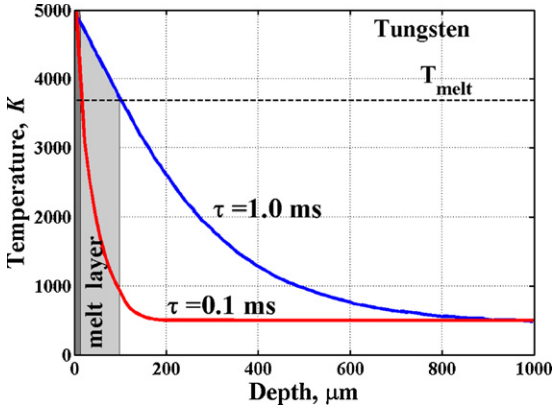

Fig. 2. Temperature distribution in W divertor at the end of heat load at giant ELM of 0.1 ms and 1 ms durations.

materials and possible plasma contamination. The long impact of plasma energy of VDE can cause melting of structure and burnout of coolant tubes. Runaway electrons penetrate deeper into first wall with Be coating and result in melting and damage of Be/Cu interface. On the other hand, W coating if possible for the first wall will protect the structural material but the tungsten armor will suffer significant melting and splashing causing.

2. Integrated simulation of plasma surface interaction during ELMs and disruptions

The large increase in both particle and heat flux, i.e., much higher than normal operation will result in significant increases in mass losses of divertor plate (vaporization, sputtering, brittle destruction, and liquid splashing). To predict these losses and potential contamination of core plasma, two main problems should be addressed, i.e., dynamics and structure of particles in scrape-off-layer (SOL) and then the interaction of particle/heat fluxes from the SOL with divertor plate materials. During ELMs [10,11], the mean free path is much larger than the connection length between parallel divertor plates and the SOL plasma becomes collisionless and has different behavior than during normal operation [12]. In the collisionless SOL plasma the edge plasma acts as an electrostatic trap for electrons. Electrons that originally have parallel energy that is lower than the wall potential energy will be trapped between the inner and outer divertor plates. To obtain the potential and corresponding net heat flux of ions and electrons to the divertor plate we used our previously developed model [12]. The ions escaping the SOL will arrive at the divertor surface with an enhanced energy due to acceleration in the negative potential nearby the plate. The ions, therefore, take part of the ELM electron energy as a result of such acceleration. This potential is less than the ambipolar one due to both the secondary electron emission at the target surface and the existing trapped electrons. Correspondingly, the incident electron energy flux decreases by the same amount needed to build up the electrostatic sheath, therefore, the total energy flux is conserved.

The density, electron temperature, and incident power for typical tokamak parameters of the major radius of 600 cm, the minor radius of 200 cm, $T_0 = 10$ keV, and $n = 10^{14}$ cm^{-3} are then calculated by solving mass conservation equation [12]. The spatial distribution of both the electron and ion heat fluxes released at midplane is calculated using HEIGHTS and have a maximum of 1.0 and 3.5 MW/cm^2 respectively.

Fig. 1 shows calculated values which then determine the hydrodynamic surface evolution of the divertor plate. Because of recent interest of using W as PFC material, we performed similar analysis of the effect of ELMs as on C and Be [12,7]. Fig. 2 shows W temperature distribution and melt-layer thickness at the end of a giant ELM ($Q_{ELM} \approx 10\%\ Q_0$) of 0.1 and 1 ms durations. Similar to C, W vaporization in case of longer giant ELM duration is low compared to Be surface. The W surface will, however, melt with thickness 100 μm developed and existing well beyond the duration of the ELM 1 ms duration. W will also have significant vaporization losses similar to C at shorter giant ELM durations with melting layer thickness of about 15 μm (Fig. 2).

Using liquid metal surfaces such as Li could be an ideal solution to accommodate plasma instabilities and the associated high heat and particle fluxes. This can be used and engineered only on areas exposed to extreme heat conditions with minimum effect on overall divertor design. Being replenishable and low-z, erosion lifetime is not a major issue and a thin layer on the divertor surface will fully protect it against giant ELMs and disruptions. For the extreme giant ELM condition with 100 μs, approximately 20 μm is needed due to vaporization to protect the surface below [7]. Because the temperature of Li surface can exceed the threshold for splashing due to bubble formation and explosion during high power ELMs, macroscopic losses in from of liquid droplets can also take place [1] and much larger Li thickness may be needed to fully protect the divertor.

However, Li vapor expansion can lead to plasma contamination even when Li erosion lifetime is not a concern. The real front of the expanding vapor cloud consists mainly of DT particles with high conductivity that results in less diffusion and, therefore, higher cloud-pressure to confine Li vapor expansion above the divertor. This can limit contamination of plasma through SOL [12]. Thus, even for giant ELMs, Li particles may not reach the separatrix through SOL during the ELM duration. On the other hand, vapor with high density and low temperature can diffuse across separatrix, nearby divertor surface, and propagate toward the X-point in dome private flux region. The Li vapor can easily diffuse toward the X-point because of both the initial low temperature nearby separatrix and decreasing of vapor temperature in dome region due to radiation. For ELM duration of about 100 μs the vapor cloud reaches the X-point with rather high density of 10^{14}–10^{15} cm^{-3} in a short time that is comparable to the ELM duration. This may mean that core contamination is possible from regions nearby the X-point. Such process of high-density vapor diffusing nearby the separatrix is less important in current tokamaks than in future high-power machines such as ITER, because of relatively low heat/particles fluxes where intense vaporization threshold depends on power load. Nevertheless, it is important to measure vapor particles concentration in dome region during ELMs in current machines to confirm above modeling results.

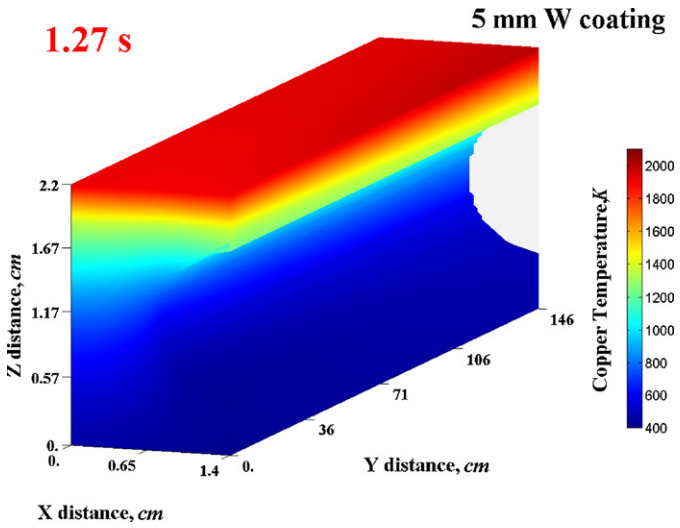

Fig. 3. Copper mockup temperature under 5-mm W coating (inlet water temperature of 413 K, water flow velocity of 20 m/s).

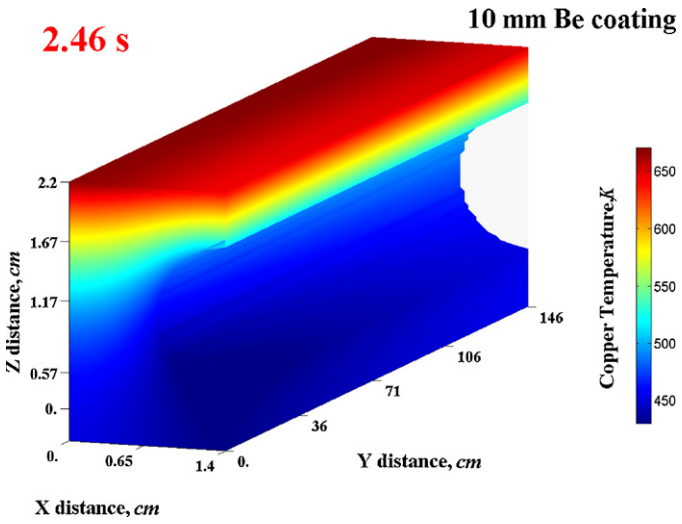

Fig. 4. Copper mockup temperature under 10-mm Be coating (inlet water temperature of 413 K, water flow velocity of 20 m/s).

3. Vertical plasma instability events and their serious damage to plasma-facing components

While plasma disruptions and ELMs will have no significant thermal effects on the structural materials or coolant channels because of their short deposition time, VDE having longer duration time [13] could have destructive impact on these components. Therefore, modeling the response of structural materials to VDE has to integrate detailed energy deposition processes, surface vaporization, phase change and melting, heat conduction to coolant channels, and critical heat flux criteria at the coolant channels. HEIGHTS 3D upgraded computer package considers all above processes to specifically study in details VDE. Time and spatial dependence of changes in water properties are taken into account when heat transfer coefficient and critical heat flux are calculated. HEIGHTS package was benchmarked against several known laboratory data and showed excellent agreement in the simulation both coating material erosion and melt-layer thicknesses for VDE transient conditions and structural material response of copper mockup for steady-state condition as well as for loss-of-flow accident and CHF criteria in smooth and swirl tubes [6].

Thermal response of ITER-like design modules to plasma VDE was studied in detail [2,6]. Results of plasma energy transient deposition of 60 MJ/m^2 over 0.5 s indicate that if the copper structure is covered by 5–10 mm tungsten or 5 mm beryllium, the heat flux to coolant channels achieves the critical value. The full 3D simulation allows detailed analysis of the structure across and along the coolant channels. Our models also take into account changing of the flow temperature along the tube. While in the case of moderate heat flux from the wall, a little increase of the water temperature at the end of the tube does not influence much on the heat exchange processes, higher thermal load from the wall along channel can significantly increase water bulk temperature and impair the water condition from being a better heat transfer media at the outlet. The critical flux values at the inlet and outlet differ significantly what determines the differences in the resulting heat exchange and wall temperatures. Exceeding of the critical heat flux (CHF) explains also cross-sectional temperature distributions where the temperature at tube area is higher than that at the edge of mockup. As the heat transfer to coolant channel is reduced, increasing local wall temperature is spread around and along the tube. More obviously this situation appears in the case of 5-mm W coating and especially in channels with swirl tape insert. Fig. 3 shows 3D temperature distribution in copper mockup, which was coated by 5-mm tungsten, at the start of coolant wall melting.

The results showed that Be coating decreases significantly the flow of incident plasma energy to copper layer and prevents copper melting even in case of 5-mm thickness where local CHF was achieved [2]. Both Be and W exhibit significant melting while Be shows much more vaporization thickness than W [6]. The large vaporization thickness of Be module and the energy removed as a result will then cause less damage to the copper structure (Fig. 4). Tungsten coating removes less plasma energy by surface vaporization and, therefore only thicker W layers – ≥15 mm – allow to reduce the heat flux intensity to sink material to ensure safe operation of copper and coolant channels [6]. Changing of coolant hydraulic parameters has little impact on copper temperatures behavior in the cases studied.

4. Self-consistent analysis of runaway electrons effect on plasma-facing components

The toroidal electric field in tokamak plasma devices gives rise to the runaway electron phenomenon during the current phase of a plasma disruption. Due to the decrease of the Coulomb collision frequency with increasing energy, electrons with energies larger than a critical threshold value are continuously accelerated by the electric field. The accelerated electrons excite waves due to the anomalous Doppler effect, i.e., a gyrating electron is similar to a flying oscillator [14]. In its coordinate system, a wave with phase velocity smaller than the electron phase velocity seems like a wave with “negative” energy. Therefore, the runaway electron can excite a wave, and increase its lateral energy and decrease its longitudinal velocity. Because of the generation of such fan type instability, the tokamak plasma initiates an oscillation burst with high-energy electron emission [15,16].

The energy deposition model was upgraded in HEIGHTS for the case of runaway electron deposition by taking into account the various interactions mechanisms of beam electrons with surface target atoms [9]. Because runaway electrons have initially relativistic energy, we included in our relativistic Monte Carlo model six main processes: (1) electron–electron scattering; (2) electron–nuclear scattering; (3) Bremsstrahlung; (4) photoabsorption; (5) Compton absorption; (6) Auger relaxation. The effect of electron–positron pair production is not included as a secondary process (after pho-

ton generation via incident electron interaction). This process is important for energy deposition of very high photons energies [17].

HEIGHTS studied energy deposition of runaway electrons on PFC for 50 MeV incident electrons energy, magnetic field inclined 1° to target surface, and impact duration 0.01 s [9]. The armor material was beryllium. The calculations were carried for different design cases for ITER assuming a total energy density of 50 MJ/m^2, magnetic field value 8 T (inboard wall), and initial temperature of all materials 100 °C. The runaway electron parameters used in this study were taken from those values predicted for ITER and future tokamak devices [18,16].

The incident angle of electrons into target depends on the Larmor spiral parameters and magnetic field direction. The Larmor radius and spiral pitch is determined from the ration of the electron kinetic energy across the magnetic field direction and the total particle kinetic energy $E_\perp/E$. Thereafter, using the term energy ratio we mean the $E_\perp/E$ ratio. Because of such complex influence, the actual incident angles of runaway electrons can be significantly different from the initial magnetic field inclination α_B that used in most present calculations. The calculations showed that the minimum molten layer thickness corresponds to the widely considered case of the electrons directed strongly along the magnetic field [9]. A runaway electrons energy ratio of 0.1 gives more than twice the molten layer thickness than the parallel case.

The angle of incidence of the magnetic field adds another peculiarity to the first wall damage response. Increasing the magnetic field angle to 4° and larger, the runaway electron energy can be deposited deep into the heat sink copper through the external beryllium armor layer [9]. HEIGHT modeling shows that for the ratio $E_\perp/E = 0.1$, electron energy 50 MeV, and impact duration 0.01 s, a melting depth of copper of up to 0.86 mm is developed in the 5° case. The beryllium armor, was not melted, however, this permits more electron heat flow to deeper layers. Therefore, magnetic field angles larger than 4° are potentially dangerous for the first wall since it can result in melting of the structure that is harder to repair compared to the armor surface materials.

To prevent melting of the heat sink and possible mitigation of the effect of runaway electrons, two solutions were proposed: increasing the beryllium thickness, or use of an additional "slowing down" layer above the heat sink structure [9]. Because beryllium is harder to use (being toxic, etc.) the second option was analyzed for the first wall heat protection. We modeled the effect of an additional tungsten layer above the copper heat think. The total size of the armor mockup is maintained constant, i.e., the beryllium layer was reduced in thickness and exchanged with an additional tungsten layer of equivalent thickness. We considered two cases of W layer location: (1) directly between beryllium and copper layers; (2) inside of beryllium layer at 0.5 cm from the top surface (at half-thickness of Be). We used in these calculations the electron energy 50 MeV, energy ratio 0.1, magnetic field inclination 5°, and impact duration 0.01 s. In the first case, the copper surface begun to melt for a tungsten layer thinner than 1 mm and the beryllium layer melts for W thickness higher than 0.5 mm. This configuration therefore does not protect the structure from melting. However, opposite to the first case, the location of the tungsten layer inside beryllium does make a difference in the structural response to the incident electrons. The safe thickness of tungsten for which all layers will remain in solid state and no melting takes place was found in range from 0.05 to 0.3 mm. Fig. 5 shows the temperature distribution as a function of the mockup depth for two cases: for 0.8 mm thickness of W layer between Be and Cu and for 0.1-thickness of tungsten inside of Be layer.

When thin W layer is located inside of Be armor, part of the deposited energy into copper is redistributed into the beryllium layer. The heat load spreads through all the mock up volume and the thermal heat wave is attenuated. The complex "sandwich" design

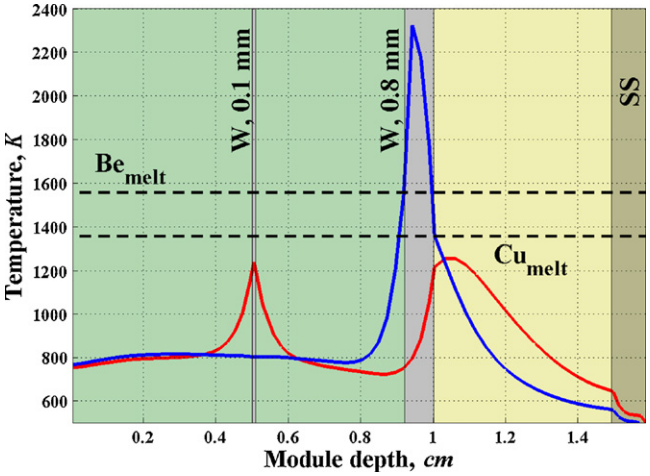

Fig. 5. Influence of tungsten layer location on Be and Cu temperature.

of the armor has the advantage of mitigating the heat load distributions in both the armor and in the structural materials. This design is complicated and requires careful manufacturing technology. However, current and advanced design technologies of fusion materials often explore various combinations of innovative bulk layers, composites, and coatings.

5. Conclusion

High power transients such as ELMs, long duration plasma instabilities such as VDEs and energetic particles such as runaway electrons are a serious concern for plasma-facing components during normal and abnormal operation of next generation tokamaks. The HEIGHTS package was updated and enhanced for the simulation and the response of PFM during major instabilities in ITER-like fusion reactors and for analyzing of methods and ways of mitigations of effects at such events.

The simulation results showed that disruptions and high power ELMs cause excessive target erosion of candidate materials such as Be, C, and W. Tungsten will start to melt for giant ELMs of energy $Q_{ELM} > 8\%\ Q_0$ and 1 ms duration. A thin layer of Li (<1 mm) can fully protect the divertor surface from giant ELMs. However, Li vapor expansion and diffusion can lead to plasma contamination even when Li erosion lifetime is not a concern.

The thermal response of ITER-like design modules to plasma VDE was also studied in detail. Results of plasma energy transient deposition of 60 MJ/m^2 over 0.5 s indicate that if the copper structure is covered by 5–10 mm tungsten or 5 mm beryllium, the heat flux to coolant channels achieves the critical value. HEIGHTS results also showed that Be coating decreases significantly the flow of incident plasma energy to copper layer and prevents copper melting even in case of 5-mm thickness where local CHF was achieved. This is simply because of the large fraction of the incident energy removed by the extensive Be vaporization. Tungsten coating removes less plasma energy by surface vaporization and, therefore only thicker W layers – $\geq$15 mm – allow to reduce the heat flux intensity to sink material to ensure safe operation of copper and coolant channels. Changing of coolant hydraulic parameters has little impact on copper temperatures behavior in the cases studied.

HEIGHTS modeled the main processes that occur during runaway electron impact. Energy deposition, material thermal response, and melting are calculated for a wide range of incident electron parameters: kinetic energy, magnetic field direction, energy ratio (along and across magnetic field direction), impact duration, and armor material. Our calculations showed that taking into account both the parallel and perpendicular electron energy

components has a significant impact on the wall armor and structural thermal response. The actual incident angle of high-energy electrons varies in a narrow range because of their spiral trajectories and the small magnetic fields inclination angle. It is shown that the standard ITER geometry of first wall with beryllium armor can melt at the interface with the structural Cu material. Using an insert of a thin tungsten layer in between the beryllium armor and Cu structure prevents melting of all structure for the parameters considered. Design optimization through computer simulation can further improve and protect future tokamak devices from runaway electron damage.

Acknowledgement

This work is supplied by US Department of Energy, Office of Fusion Energy Sciences.

References

[1] A. Hassanein, Prediction of material erosion and lifetime during major plasma instabilities in tokamak devices, Fusion Eng. Design 60 (2002) 527.
[2] A. Hassanein, T. Sizyuk, M. Ulrickson, Vertical displacement events: a serious concern in future ITER operation, Fusion Eng. Design 83 (2008) 1020.
[3] A. Hassanein, Fusion Technol. 30 (1996) 713.
[4] A.R. Raffray, G. Federici, J. Nucl. Mater. 244 (1997) 85.
[5] A. Hassanein, G. Federici, I. Konkashbaev, A. Zhitlukhin, V. Litunovsky, Fusion Eng. Design 39–40 (1998) 201.
[6] A. Hassanein, T. Sizyuk, Comprehensive simulation of vertical plasma instability events and their serious damage to ITER plasma facing components, Nucl. Fusion 48 (2008) 115008.
[7] A. Hassanein, T. Sizyuk, I. Konkashbaev, Integrated simulation of plasma surface interaction during edge localized modes and disruptions: self-consistent approach, J. Nucl. Mater. 390–391 (2009) 777–780.
[8] A. Hassanein, I. Konkashbaev, Comprehensive physical models and simulation package for plasma/material interactions during plasma instabilities, J. Nucl. Mater. 273 (1999) 326.
[9] V. Sizyuk, A. Hassanein, Self-consistent analysis of the effect of runaway electrons on plasma facing components in ITER, Nucl. Fusion 49 (2009) 095003.
[10] A.V. Chankin, N. Asakura, T. Fukuda, A. Isayama, Y. Kamada, Y. Miura, et al., Fast ELM dynamics in JT-60U, Nucl. Fusion 42 (2002) 733–742.
[11] A. Loarte, G. Saibene, R. Sartori, D. Campbell, M. Becoulet, L. Horton, et al., Characteristics of type I ELM energy and particle losses in existing devices and their extrapolation to ITER, Plasma Phys. Control. Fusion 45 (2003) 1549–1569.
[12] A. Hassanein, I. Konkashbaev, Comprehensive modeling of ELMs and their effect on plasma-facing surfaces during normal tokamak operation, J. Nucl. Mater. 313–316 (2003) 664.
[13] M. Merola, M. Rödig, J. Linke, R. Duwe, G. Vieider, Behaviour of plasma facing materials under VDE, J. Nucl. Mater. 258–263 (1998) 653–657.
[14] M. Einat, E. Jerby, Phys. Rev. E 56 (1997) 5996.
[15] R.D. Gill, B. Alper, A.W. Edwards, L.C. Ingesson, M.F. Johnson, D.J. Ward, Nucl. Fusion 40 (2000) 163.
[16] Z.Y. Chen, B.N. Wan, S.Y. Lin, Y.J. Shi, L.Q. Hu, Phys. Lett. A 351 (2006) 413.
[17] J.H. Hubbell, H.A. Gimm, I. Overbo, J. Phys. Chem. Ref. Data 9 (1980) 1023.
[18] G. Maddaluno, G. Maruccia, M. Merola, S. Rollet, J. Nucl. Mater. 313–316 (2003) 651.